Main manuscript for

Synthesis of Palladium Nanoparticles by Electrode-Respiring *Geobacter sulfurreducens* Biofilms

Marko S. Chavez[a]*, Magdalene A. MacLean[a], and Mohamed Y. El-Naggar[a,b,c]

[a]Department of Physics and Astronomy, University of Southern California, Los Angeles, CA, 90089, USA; [b]Department of Biological Sciences, University of Southern California, Los Angeles, CA, 90089, USA; [c]Department of Chemistry, University of Southern California, Los Angeles, CA, 90089, USA

*To whom correspondence should be addressed
University of Southern California, 1002 Childs Way, MCB 230, Los Angeles, CA 90089-3502
Email: mschavez@usc.edu

Abstract

The electroactive microorganism *Geobacter sulfurreducens* can couple organic electron donor oxidation to the respiration of electrode surfaces, colonizing them in the process. These microbes can also reduce soluble metal ions, such as soluble Pd, resulting in metallic nanoparticle (NP) synthesis. Such NPs are valuable catalysts for industrially relevant chemical production; however, their chemical and solid-state synthesis are often energy intensive and result in hazardous biproducts. Utilizing electroactive microbes for precious metal NP synthesis has the advantage of operating under more sustainable conditions. By combining *G. sulfurreducens*' ability to colonize electrodes and synthesize NPs, we performed electrode cultivation ahead of biogenic Pd(0) NP synthesis for the self-assembled fabrication of a biohybrid cell-Pd material. *G. sulfurreducens* biofilms were grown in electrochemical reactors with added Pd(II), and electrochemistry, spectroscopy, and electron microscopy were used to confirm (1) metabolic current production before and after Pd(II) addition, (2) simultaneous electrode respiration and soluble Pd reduction over time, and (3) biofilm-localized Pd NP synthesis. Utilizing electroactive microbes for the controlled synthesis of NPs can enable the self-assembly of novel cell-nanoparticle biohybrid materials with unique electron transport and catalytic properties.

Keywords: Biofilms; Biomineralization; Palladium nanomaterials; Biohybrid materials; Microbial electrochemistry; Extracellular electron transport

Synopsis

Simultaneous electrode respiration and soluble Pd reduction by *G. sulfurreducens* biofilms enables biofilm-localized Pd(0) nanoparticle formation.

Introduction

Electroactive microbes can couple the oxidation of organic electron donors to the respiration of external solid minerals as well as electrode surfaces in a process referred to as extracellular electron transport (EET)[1,2]. To overcome the hurdle of electron transport at this biotic-abiotic interface, these microorganisms utilize a series of multiheme cytochromes that carry charge from the inner membrane to the outer membrane, and then ultimately to external surfaces[3–6]. In the model electroactive bacterium *Geobacter sulfurreducens*, a suite of inner membrane, outer membrane, and excreted cytochromes enable it to perform EET with a variety of external electron acceptors [7–11]. When cultivated on electrode surfaces, individual *G. sulfurreducens* cells form current producing biofilms tens of microns thick, with these biofilms being made up of on the order of tens of cell layers, with the ability to produce up to approximately 1 mA/cm^2 of current [12]. In addition to electrode respiration and cultivation, *G. sulfurreducens* is reported to also be capable of using its multiheme cytochromes to reduce metal ions such as soluble Pd for the biomineralization of elemental Pd nanoparticles (NPs) [13–17].

Pd nanomaterial synthesis specifically is of interest as Pd serves as an important catalyst harnessed for decades by pharmaceutical and agricultural industries to produce technological relevant chemicals[18]. Additionally, because of the waste runoffs of such industries, soluble Pd reclamation is of environmental interest as its recollection limits its toxic presence in the environment and enables the reuse of Pd catalysts[19]. However, current solid-state and chemical methods for Pd synthesis and reclamation remain energy intensive and give off hazardous chemical waste biproducts[19,20]. In contrast, electroactive microbes can interact with a diverse range of metal and chalcogen ions, for energy generation and detoxification, leading to the precipitation of

technological relevant nanomaterials, including Pd nanoparticles by *G. sulfurreducens*, under physiological temperature, pressure, and pH[21–25]. Thus, biomineralization does not require expensive fabrication equipment, harsh environmental conditions, nor does it produce the harmful chemical waste of traditional solid-state and chemical fabrication methods [25,26]. Semiconductor nanomaterials biomineralized by electroactive microbes have recently been harvested and used in the fabrication of functional field-effect transistors, while metallic biofabricated nanoparticles have been used as catalysts to drive industrially relevant chemical processes [21,27]. Electroactive microbes used in some previous biomineralization work have also been genetically modified, allowing experimenters to tune the morphology and optical properties of biomineralized semiconductor nanomaterials [28,29]. So far, with a few exceptions, many biomineralization studies using electroactive microorganisms have been performed with planktonic cell cultures, where individual cells are free floating in media, rather than in biofilm containing cultures[30]. Specifically, to the best of the authors' knowledge, all previous studies of Pd NP synthesis by *G. sulfurreducens* have focused on planktonic cells[21–25]. More recently, utilizing *Shewanella oneidensis*, another electroactive model organism, biofilm-localized Pd nanomaterial formation was used for the construction of self-assembled hybrid Pd-cell biomaterials capable of catalyzing chromium reduction for water detoxification. This work highlights the importance of biofilm-localized NP synthesis for localized material formation in biohybrid film synthesis. The study also discusses how biofilms, which are more robust in the face of toxins than single cells, could enable higher NP production rates by protecting the biomass from the toxic effects of metal ions during material synthesis[31,32].

Building on previous works that harnessed planktonic *G. sulfurreducens* cells for nanomaterial synthesis, we characterize the soluble Pd reduction capabilities of actively electrode-respiring *G. sulfurreducens* PCA biofilms for the first time for the self-assembly of a biohybrid cell-Pd nanomaterial film. In bioelectrochemical reactors, biofilms were cultivated on graphite working electrodes (WE) and on Au interdigitated array (IDA) WEs. Cyclic voltammetry (CV) scans were performed at various time points to show the viable electrochemical activity of the biofilms before and after Pd(II) addition. Inductively coupled plasma optical emission spectroscopy (ICP-OES) was used to monitor the soluble Pd concentration over time in these reactors and in relevant controls to show *G. sulfurreducens* biofilms were indeed capable of simultaneously respiring WEs and reducing soluble Pd. And finally, scanning electron microscopy (SEM) and energy dispersive spectroscopy (EDS) was used to confirm that after the addition of Pd(II) into *G. sulfurreducens* reactors, precipitated Pd NPs were localized to the surface of biofilms cultivated both on graphite and Au IDA WEs, leading to the creation of a biohybrid cell-Pd nanomaterial film. This work adds to the collection of very few studies investigating the biomineralization capabilities of electrode-respiring biofilms. The resulting self-assembled biohybrid materials may be able to be used for their possible unique electrical or catalytic properties. Additionally, by taking advantage of other cell localization strategies, moving forward, biofilm patterning and biofilm-driven biomineralization could be combined for the spatially controlled deposition of biogenic nanomaterials in more complex geometries.

Experimental Section

Cell growth protocols. From a frozen dimethyl sulfoxide (DMSO) stock, *Geobacter sulfurreducens* PCA was streaked out onto plates of semisolid (1% agar, v/v) defined medium (referred to as NB medium), with added 20 mM sodium acetate and 40 mM fumaric acid, under an $N_2/CO_2/H_2$ (75:20:5) atmosphere in an anaerobic chamber (Bactron 300, Sheldon

Manufacturing Inc.) and incubated at 30°C. NB medium supplemented with fumaric acid and sodium acetate is referred to as NBFA. NB medium supplemented with only acetate is referred to as NBA. Under the $N_2/CO_2/H_2$ atmosphere of an anerobic chamber, single colonies were plucked from the streaked plates and were used to inoculate microcentrifuge tubes containing 1 mL of NBFA. The microcentrifuge tubes were then incubated at 30°C. Once thick red clouds of cells were observed in the microcentrifuge tubes, typically after about three days of incubation, the contents were transferred to sterile, anaerobic serum tubes containing 10 mL of NBFA, referred to as NBFA1. Newly inoculated NBFA1 tubes were removed from the anaerobic chamber and placed in a 30°C incubator with no agitation. Growth was measured in the serum tubes by the culture optical density at 600 nm (OD_{600nm}) using a spectrophotometer (VWR V-1200 Spectrophotometer). At stationary phase, about OD_{600nm}: 0.7, 1 mL of each NBFA1 was used to inoculate a second set of sterile, anaerobic serum tubes containing 10 mL NBFA, referred to as NBFA2. NBFA2 tubes were incubated at 30°C with no agitation and at late log phase, about OD_{600nm}: 0.6, 10 mL of the NBFA2 tubes were used to inoculate sterile, anaerobic reactors already containing 10 mL of NBA, for a final inoculated reactor volume of 20 mL.

Defined NBFA media recipe. Per liter, the defined NB medium consisted of 0.38 g KCl, 0.2 g NH_4Cl, 0.069 g $NaH_2PO_4 \cdot H_2O$, 0.04 g $CaCl_2 \cdot 2H_2O$, 0.2 g$MgSO_4 \cdot 2H_2O$, and 10 mL of trace minerals mix. Per liter, the trace mineral mix contained 1.5 g $C_6H_6NNa_3O_6$, 0.1 g MnCl2·$4H_2O$, 0.5 g $FeSO_4 \cdot 7H2O$, 0.17 g $CoCl_2 \cdot 6H_2O$, 0.1 g $ZnCl_2$, 0.03 g $CuSO_4 \cdot 5H_2O$, 0.005 g $AlK(SO4)_2 \cdot 12H_2O$, 0.005 g H_3BO_3, 0.09 g Na_2MoO_4, 0.05 g $NiCl_2$, 0.02 g $NaWO_4 \cdot 2H2O$, and 0.10 g Na_2SeO_4. The medium was adjusted to a pH of 6.8 with NaOH before 2.0 g of $NaHCO_3$ was added. All serum tubes and bottles used in *G. sulfurreducens* experiments were degassed using N_2/CO_2 (80:20), passed over a heated copper column to remove trace oxygen, for ten minutes (tubes) and 30 minutes (bottles) before being sealed with butyl rubber stoppers and autoclaved.

Bioelectrochemical reactor construction for anaerobic electrochemistry.
The bioelectrochemical reactor (referred to just as reactor) design used in this work was adapted from the *G. sulfurreducens* reactors used in the Daniel Bond Laboratory at the University of Minnesota-Twin Cities[33]. The reactors consisted of glass cones (BASi MF-1084) where their openings were sealed between custom polyether ether ketone (PEEK) plastic rings and lids. The lids contained electrode, gas exchange, and sampling ports. The lids were screwed shut with rubber O-rings sandwiched between the lids and the rim of the glass cones to maintain an airtight seal. The reference electrode (RE) connections consisted of glass tubes (6-8 cm long, with a 4 mm outer diameter) with porous glass frits heat sealed to the ends and with syringes, without their plungers, connected to the other ends. The counter electrodes (CEs) consisted of Pt wires (at least 2.5 cm long, with a 0.25 mm diameter) with one end sealed within glass tubes and soldered, inside the glass, to copper wires extending out of the other end of the tubes. Two different types of working electrodes (WEs) were used. For assessing the initial capabilities of *G. sulfurreducens* to remain electrochemically active following Pd(II) addition and to simultaneously respire an electrode surface and reduce soluble Pd, polished graphite electrodes were used, with surface areas of 3 cm^2. To confirm biofilm-localized Pd nanoparticle formation could occur when *G. sulfurreducens* was grown on a different type of electrode, Au interdigitated array (IDA) electrodes (ALS Japan 012125), with a surface area of 0.026 cm^2, were also used as the reactor working electrodes (WEs).

Graphite electrodes were polished on each face with 1500 grit sandpaper and then sonicated in DI water at least three times for ten minutes. The spent DI water was exchanged for fresh DI

water between each sonication. WE connecters for the polished graphite were constructed in the same way as the Pt CEs, except a Pt loop was exposed at one end of a glass tube instead of a free hanging Pt wire. After sonication, the graphite electrodes were screwed onto the Pt loops of the WE connectors through a hole in the electrodes, using nylon nuts (Grainger model: 4AGF1) and bolts (Grainger model: 4DFJ6). The Au IDAs consisted of 65 pairs of interdigitated electrode fingers where each pair was separated by a 5 μm gap and each electrode finger was 10 μm wide and 2 mm long. The IDA electrodes, except for the interdigitated area and the contact pads, were passivated with a polymer layer. To wire the IDAs, the exposed ends of two thin, insulated copper wires were silver painted (Product number: 16035 TED PELLA, Inc.) onto the two WE contact pads of the IDAs. Then, the contact pad area was sealed with insulating resin (3M Scotchcast Flame-Retardant and Electrical Insulating Compound 2131).

The PEEK parts and the glass cones for the reactors were soaked in 4 M HCl for at least 24 hours and then rinsed in DI water before being used. O-rings and plastic gas inlet and outlet fittings were rinsed and then soaked in DI water for at least 24 hours before being used. Assembled reactors, with the RE connectors removed, were filled alternatingly with 1 M NaOH and then 1 M of HCl. This was done three times for each solvent, with a ten-minute soaking time. The RE connectors were then inserted into the reactors prior to the final 1 M HCl soak. The reactors were then rinsed and filled with DI water, lightly sealed, and then autoclaved. For experiments using the Au IDAs as working electrodes, the electrodes were left out of the above cleaning and sterilization procedure. To sterilize the IDAs, they were carefully dipped into 10% bleach for 10 seconds such that only the interdigitated area of the IDAs were submerged. Then, the interdigitated area of the IDAs was dipped into sterile DI water for 20 seconds. Finally, the entire IDA electrode, including the part covered in resin, was rinsed with sterile DI water. The IDA wires were also wiped with sterile DI water. At a laminar flow bench, after autoclaving, the reactors were opened and the cleaned and wired IDAs were carefully inserted in. The reactors were then resealed.

After sterilization, and after WE insertion in the cases where the IDAs were used, a solution of 1 % agar and 0.1 M Na_2SO_4 was heated and then carefully added into the RE connectors using a long metal needle, to act as a salt bridge. Once the salt bridge solidified, 1 mL of 1 M Na_2SO_4 was added on top of it. The DI water in the reactors was removed through the sampling port and 10 mL of sterile, anaerobic NBA medium was added to each reactor. The reactors were then set to purge with N_2/CO_2 (80:20) flowing over a heated copper column to remove trace oxygen. The gas also passed through a 0.2 μm filter and an anaerobic (N_2/CO_2), sterile DI water containing humidifier serum bottle before entering each reactor. A consistent flow of N_2/CO_2 through the reactors was maintained for the duration of all electrochemical experiments.

Microbial electrochemistry and Pd(II) addition workflow. Microbial electrochemistry was used to investigate whether *G. sulfurreducens* biofilms could remain electrochemically active following Pd(II) addition and if they were capable of simultaneously respiring an electrode and reducing added Pd(II). Once N_2/CO_2 had been flowing through the reactors for at least an hour, 1 M KCl Ag/AgCl reference electrodes (REs) were rinsed with ethanol and DI water and then placed into the 1 M Na_2SO_4 electrolyte on top of the salt bridges in each reactor RE connector. Note: all potentials listed in this manuscript are vs 1 M KCl Ag/AgCl unless stated otherwise. A four channel Squidstat potentiostat (Admiral Instruments, Inc.) was used for all chronoamperometry (CA) measurements and for cyclic voltammetry (CV) measurements performed on the graphite electrode reactors. Sterile, cell-free NBA medium cyclic voltammetry (CV) scans were performed on each graphite electrode reactor after they achieved a sufficiently anaerobic environment. In the

case where IDA working electrodes were used, sterile, cell-free NBA medium electrochemical gating scans were performed, instead of CV scans, using two Gamry Reference 600 potentiostats linked with a synchronization cable and operating in bipotentiostat mode. CA scans were started immediately after the cell-free CV scans. For all CV scans, the working electrodes (WE) were scanned between -0.650 V and 0.350 V for three cycles at a scan rate of 1 mV/sec. For the case where IDAs working electrode were used, the same parameters were used, except there was a 20 mv gating offset applied between the two electrodes. For all CA scans, the WE potentials were held fixed at 0.3 V. For the case where IDAs were used as the working electrodes, the two WEs were shorted together and held at 0.3 V during the CAs. Once CA current reached a steady background value in sterile, cell-free NBA media, the reactors were inoculated with 10 mL of late log *G. sulfurreducens*. For graphite electrode biofilm cultivation, reactor stir bars were set to about 1000 RPM and left stirring during all CV scans. For the IDA electrode biofilm cultivation, stir bars were set to about 200 RPM and were turned off during gating scans as the stirring affected the measurement.

Inductively coupled optical emission spectroscopy (ICP-OES) for monitoring soluble Pd reduction. ICP-OES samples were collected from reactors and sterile media bottle control experiments over time to monitor soluble Pd reduction. One to two mL of solution was removed periodically from the reactors or bottles after the addition of 0.5 mM Na_2PdCl_4, with the first sample being taken immediately after the addition of Pd(II). The removed samples were then 0.2 μm filtered, placed into cryovials or microcentrifuge tubes, and then frozen at -20°C to prevent unwanted chemical reactions from occurring before the ICP measurements could be made. Before ICP measurements, the samples were thawed at room temperature and then suspended in 5% HCl. A series of standard soluble Pd concentrations spanning the range of concentrations expected were created by diluting a stock ICP standard Pd solution (Product number: 77091 Millipore Sigma). All samples and standards were suspended in a final concentration of 5% HCl to ensure the Pd was soluble and matched the HCl concentration of the undiluted stock ICP standard Pd solution. A Thermo Fischer iCAP 7400 ICP-OES was used for all these measurements.

Scanning electron microscopy and energy dispersive spectroscopy for the observation and elemental analysis of biofilm-localized palladium nanomaterial formation. To confirm biofilm-localized Pd nanoparticle formation, scanning electron microscopy (SEM) and energy dispersive spectroscopy (EDS), were used. All biofilm-electrode SEM and EDS samples underwent a series of ethanol dehydrations followed by critical point drying so that the cells did not deform under vacuum. Working electrodes (WEs) were submerged in 25% ethanol for 15 minutes, 50% ethanol for 15 minutes, 75% ethanol for one hour, and 100% ethanol for at least 15 minutes. The WEs were then subjected to critical point drying using a Tousimis Autosamdri-815. Imaging was performed with either a JEOL JSM 7001F SEM or an FEI Nova NanoSEM 450. Elemental analysis was performed with a JEOL JSM 7001F SEM using an accelerating voltage of 9 kV and a probe current of 12.

Results and Discussion

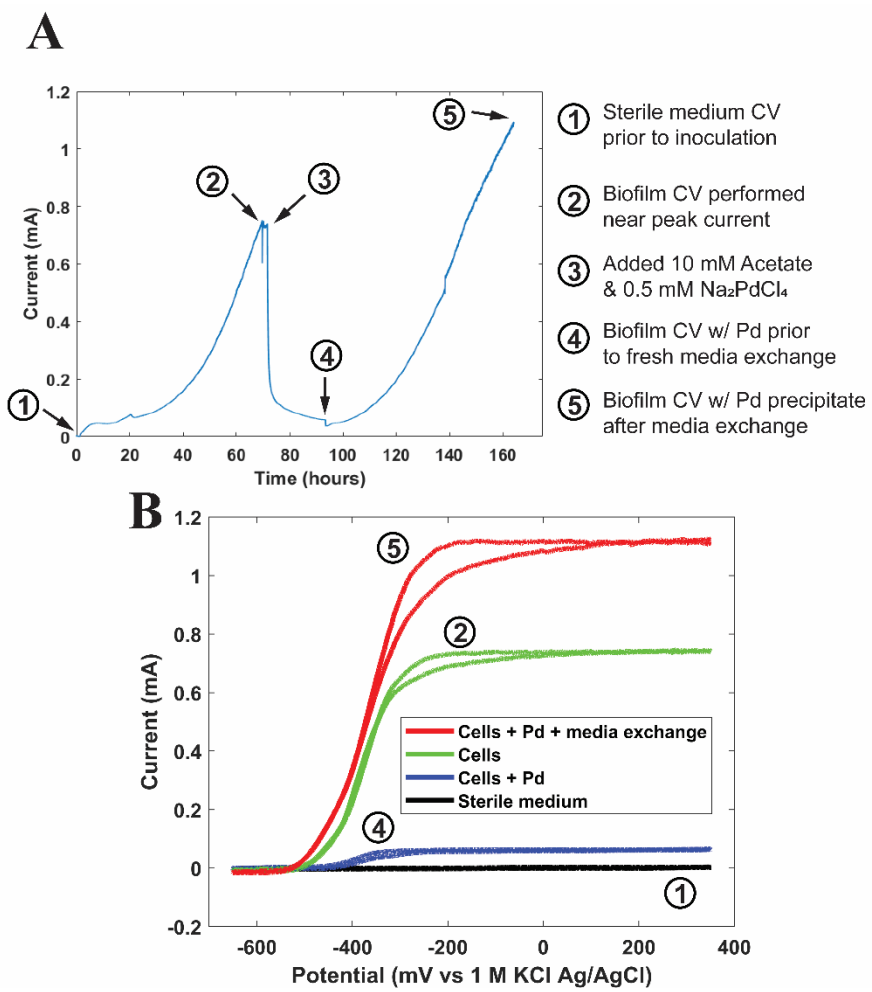

Figure 1. Representative chronoamperometry and cyclic voltammetry, of a triplicate set, taken before and after Pd(II) addition to the *G. sulfurreducens* reactors. (A) Chronoamperometry shows current production throughout the biofilm cultivation and Na_2PdCl_4 addition experiment. Workflow is identified by number markers. (B) Cyclic voltammetry shows that while current production changes throughout the Pd(II) addition experiment, the electron transport at the electrodes observed in (A) is metabolic in nature, with the midpoint potential of the voltammograms occurring at the formal potential of outer membrane *G. sulfurreducens* cytochromes. Markers in (B) correspond to the time points marked in (A) when those voltammograms were taken.

***G. sulfurreducens* biofilms can retain electrochemical activity following Pd(II) addition.** To determine if *G. sulfurreducens* biofilms remained electrochemically active following the addition of Pd(II) to reactors, we first cultivated cells in anaerobic reactors on graphite working electrodes (WEs) with the electrodes acting as the sole electron acceptors in the culture. Chronoamperometry (CA) was performed to monitor the current produced by the cells as the biofilms formed on the WEs. In a CA scan, the potential of a working electrode in an electrochemical reactor is held at a fixed potential that is favorable for electron transport between an electroactive microbe and the WE, allowing for electrode cultivation[33]. Here, current was used as an approximate indicator of cell viability and biofilm growth [33–35]. As current production began to plateau, cyclic voltammetry (CV) scans were performed to assess the electrochemical activity of the biofilm prior to adding Pd(II). In a CV scan, the potential of the WE in an electrochemical reactor is swept across a defined range while current is measured at the WE, giving mechanistic information about the WE electron transport[33,36]. About 24 hours after adding Pd(II), a CV scan was performed again to assess the

activity of the biofilm following the expected reduction of the added Pd(II). A Pd-free media exchange was then performed to see if any toxic affects experienced by the biofilm after the Pd(II) addition step could be removed. A final CV scan was then performed to assess the activity of the biofilm after the media exchange. A simplified workflow overview is listed on the right in Figure 1A.

In Figure 1A, in between markers 1 and 2, we observed an exponential increase in current after inoculation, indicating an exponential phase in cell growth and biofilm formation at the WEs. At the time point indicated by marker 2, the green CV scan in Figure 1B shows the expected metabolic activity of *G. sulfurreducens* biofilms as they respire the provided electrodes to gain energy. Here, the observed sigmoidal shape of the CV indicates acetate (electron donor) oxidation is couple to electrode (electron acceptor) respiration[37]. Additionally, the green CV scan confirms that the electrode respiration is occurring at the formal potential of the *G. sulfurreducens* extracellular electron transport (EET) proteins as the center of the wave shaped portion of the plot is around -400 mV vs 1 M KCl Ag/AgCl[38]. In Figure 1A, after the addition of Pd(II) at marker 3, current was observed to first sharply decrease and then to slowly decrease over 24 hours to approximately 10% of the original value. With the known initial added Pd(II) concentration and the time for complete soluble Pd reduction (Figure 2), and assuming the soluble species is Pd(II), the amount of current needed for this reaction was calculated to be on the order of 600 uA, roughly 75% of what the biofilm was producing just prior to the Pd(II) addition. This indicates that the immediate loss in current observed upon Pd(II) addition could be due to the soluble Pd acting as an alternate electron sink. However, since there is also a persistent loss in current lasting many hours after the complete reduction of the soluble Pd, there could be an additional toxic effect of the soluble Pd on the biofilm, as metal ions can be harmful to microbes above certain quantities which vary by organism [39,40]. Thus, the addition of Pd(II) into the reactors resulted in a dramatic loss in electrochemical activity that could either be due to the soluble Pd acting as an alternate electron sink or due to inhibition of activity. Since 10 mM of sodium acetate was added to the reactors along with the Pd(II), the observed drop in current was not due to electron donor limitation. The blue CV scan in Figure 1B taken 24 hours after Pd(II) addition and immediately before the media exchange still shows that electrode reduction is taking place at the formal potential of the cells' EET proteins, however, the decrease in current magnitude reflects the hinderance in EET seen between markers 3 and 4 in Figure 1A.

After the media exchange at marker 4 in Figure 1A, current was observed to increase exponentially. This increase in current as well as the CV scan performed at marker 5 in Figure 1A and displayed in red in Figure 1B shows that the media exchange was able to restore the electrochemical activity lost after the addition of Pd(II). This recovery following a media exchange shows that the soluble Pd-associated inhibition in biofilm current production did not cause long-term issues in electrochemical activity. Here, the implementation of electrochemistry enabled a real-time readout of cell activity before and after Pd(II) addition, allowing us to observe how cells were affected by the soluble Pd and the subsequent media exchange. From our results, we show that *G. sulfurreducens* biofilms can recover electrochemical activity following Pd(II) addition. Additionally, as discussed in the introduction, the data suggest that our biofilms acted to protect the cells after Pd(II) addition, albeit with reduced activity, allowing for the observed recovery following a change to more favorable conditions.

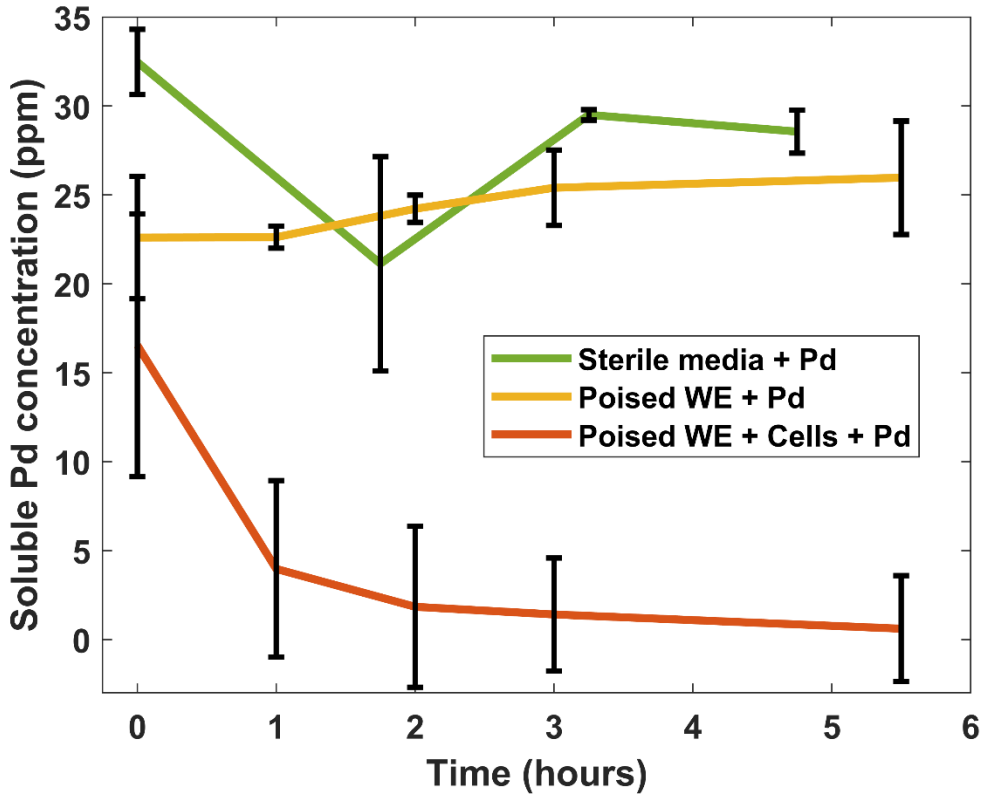

Figure 2. Soluble Pd concentration measured over time via inductively coupled plasma optical emission spectroscopy (ICP-OES) in sterile NBA media, in a cell-free reactor with sterile NBA media and a poised working electrode (WE), and in an electrochemical reactor where a biofilm was cultivated on the electrode. The soluble Pd concentrations displayed at each time point are an average of a triplicate set and the error bars represent the standard deviation of that triplicate set. 0.5 mM Na_2PdCl_4, approximately 50 ppm, was added to each condition and the first time point was taken immediately after the addition of the Pd(II).

***G. sulfurreducens* biofilms are capable of simultaneous electrode respiration and soluble Pd reduction.** Between the timepoints indicated by markers 3 and 4 in Figure 1A, small volumes of solution were periodically taken from *G. sulfurreducens* reactors after the addition of 0.5 mM Na_2PdCl_4 to monitor the concentration of soluble Pd as a function of time via inductively couple plasma optical emission spectroscopy (ICP-OES). As controls, 0.5 mM Na_2PdCl_4, was added to sterile media in anerobic bottles and to sterile, cell-free reactors with the WEs held at the biofilm cultivation potential of 0.3 V. The initial concentration of 0.5 mM Na_2PdCl_4 is roughly equal to 50 ppm of Pd(II). In the control experiments, small volumes of the solution were also periodically removed to monitor the soluble Pd concentration over time, also via ICP-OES. These cell and cell-free soluble Pd reduction measurements were performed in triplicate. In Figure 2, while there was an initial drop in soluble Pd concentration observed in all cases, only for the case where a biofilm was present was there a complete reduction of the added soluble Pd over time. In the two control cases, after the initial concentration drop, the concentration of soluble Pd remained roughly constant over the same timescale during which the biotic condition removed the soluble Pd. The initial drop in concentration could be due to some abiotic reduction of soluble Pd by media components. Since the biofilm-based soluble Pd reduction took place while partial current production was still observed in the chronoamperometry and since metabolic electrode reduction could be observed in the cyclic voltammogram after soluble Pd removal, we conclude that *G.*

sulufurreducens biofilms are capable of simultaneously respiring electrodes and reducing soluble Pd in solution. In a previous study where planktonic *G. sulfurreducens* were used for Pd NP synthesis, NPs were separated from cell cultures following synthesis and the cells were reused in Pd NP synthesis[13]. Since we show that our biofilms recover electrochemical activity following soluble Pd reduction, they could similarly potentially be used in subsequent soluble Pd removal experiments.

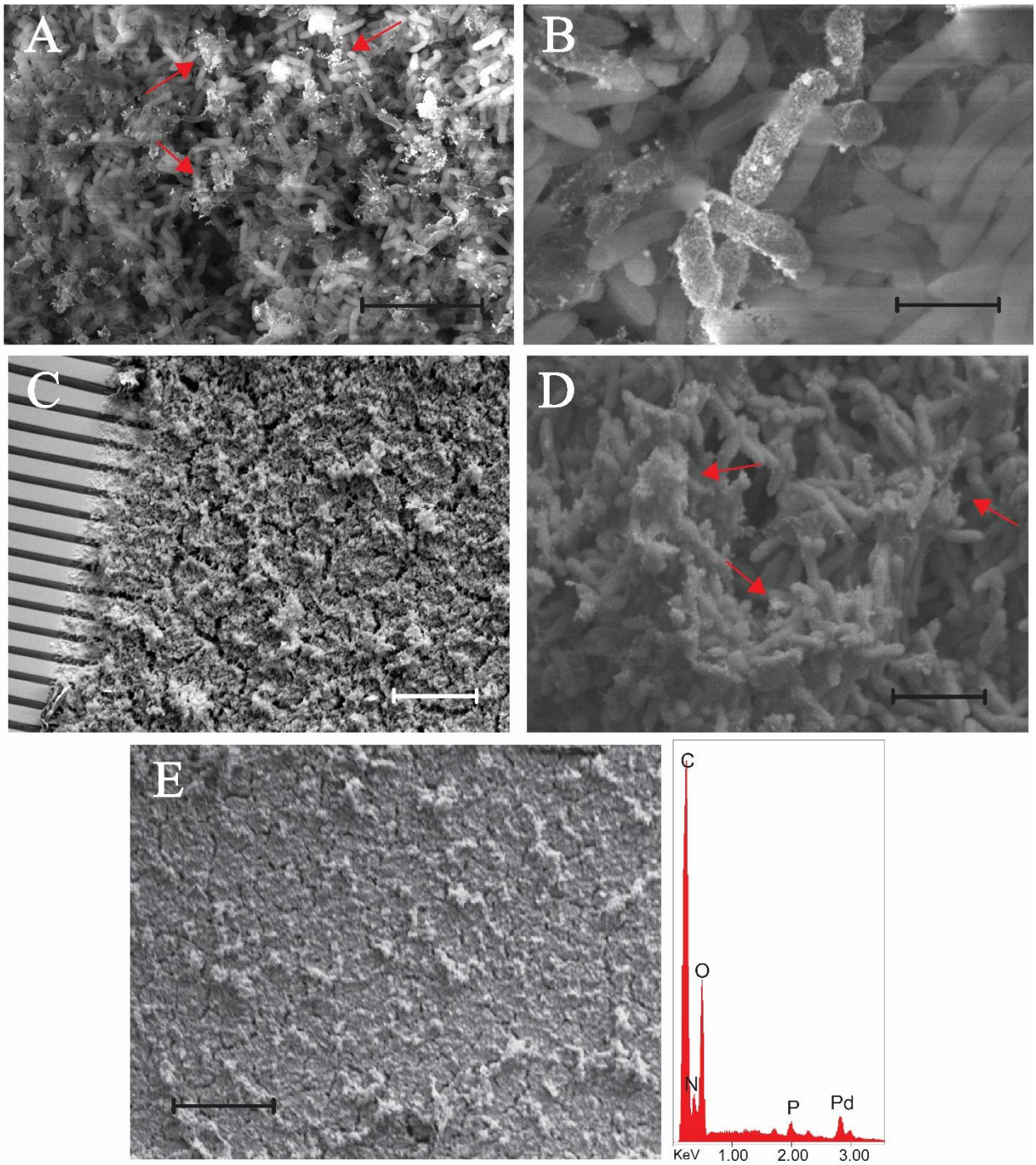

Figure 3. Representative scanning electron microscopy (SEM) and an energy dispersive spectroscopy (EDS) spectrum for *G. sulfurreducens* biofilms following biogenic soluble Pd reduction. (A) Zoomed out and (B) zoomed in SEM image of *G. sulfurreducens* grown on a graphite electrode with added Pd(II). The Pd NPs, some identified with red arrows, appear as white spheres unevenly peppering the biofilm. (C) Zoomed out and (D) zoomed in SEM image of *G. sulfurreducens* grown on an Au interdigitated array (IDA) electrode. The Au bands of the IDA can be seen to the left of the biofilm in (C). In (D), spherical Pd NPs can be observed, some identified with red arrows, encrusting the cells in the biofilm on the IDA. (E) A different location of the same biofilm shown in (C) and (D) where the EDS spectrum (arbitrary unit y-axis) shows that Pd is present throughout the surface. (A) Scale bar is 5 μm. (B) Scale bar is 1 μm, (C) Scale bar is 50 μm. (D) Scale bar is 2 μm. (E) Scale bar is 50 μm.

Biofilm-based soluble Pd reduction enables localized Pd(0) nanoparticle biomineralization. Following the electrochemical measurements, the working electrodes (WEs) were analyzed via scanning electron microscopy (SEM) and energy dispersive spectroscopy (EDS) to confirm biofilm-localized Pd nanoparticle formation resulting from the soluble Pd reduction by the *G. sulfurreducens* biofilms. In both the graphite and IDA experiments, a dense biofilm was observed on the WEs (Figure 3A and 3C). This is expected as *G. sulfurreducens* is known to form tens of microns thick biofilms on electrode surfaces [12]. In these images, Pd nanoparticles (NPs) appear as bright white precipitate and can be observed decorating the cells within the biofilms. Zoomed in images show that some of these precipitate-crusted cells are completely covered in NPs with diameters on the order of less than 10 nanometers (Figures 3B and 3D). These images confirm that the biofilm-based soluble Pd reduction observed in the results of the previous section resulted in biofilm-localized Pd NP precipitation. However, in these images, an uneven distribution of Pd NPs can be seen, with some cells completely covered in nanomaterials while some are uncovered or sparsely covered. This could be due to uneven activity of cells on the biofilm surface, as seen in experiments that mapped metabolic activity of *G. sulfurreducens* cells as a function of their position in electrode grown biofilms [12]. Biofilm roughness at the solution-facing surface as well as the ability of soluble Pd to diffuse to that biofilm surface could have resulted in varied soluble Pd exposure at the cell-solution interface.

To confirm the presence of Pd more directly, EDS was used to perform elemental analysis on a precipitate crusted IDA grown biofilm. An EDS spectrum was collected from a large, about 200 μm by 300 μm, region of the IDA grown *G. sulfurreducens* biofilm (Figure 3E). From the EDS spectrum, Pd was detected in the scanned region of the biofilm. The additional elemental peaks observed (e.g. C, N, O, and P) are expected as they are essential building blocks of living organisms as well as essential components of the growth media [41]. These results further confirm that Pd NP formation did occur at the biofilm surface and that it occurred over a large region of the biofilm. Following the electrochemistry and ICP-OES results, our SEM and EDS analysis confirm the biogenic synthesis of Pd nanoparticles by electrode cultivated biofilms enables localized nanomaterial formation on cells.

Conclusions

From our electrochemical measurements, we showed that *G. sulfurreducens* biofilms were capable of simultaneously respiring WEs and reducing soluble Pd, where partial EET capability was observed after Pd(II) addition and full EET capability was restored following a media exchange. Additionally, we showed that the biofilm presence within the electrochemical reactors is required for the complete removal of the added Pd(II). Finally, from our electron microscopy results, we showed that following soluble Pd reduction, Pd NPs had precipitated onto the surface of *G. sulfurreducens* biofilms cultivated on either graphite or Au interdigitated array (IDA) WEs, confirming biofilm-localized nanomaterial biomineralization. With these results, we expand on what little work has been done on electroactive biofilm-based metal ion reduction and biomineralization. This work has applications in localizing biomineralized nanomaterials for the construction of hybrid metal-cell biomaterials for potential uses in catalysis[31]. With localized Pd NP biomineralization observed on a *G. sulfurreducens* biofilm cultivated on an IDA, this process could also be used for biofilm doping with potential applications in modifying the conduction and catalytic activity of biofilm-based microbial electrochemical energy systems[42,43]. Additionally, combining the biofilm-based controlled nanomaterial synthesis discussed here with biofilm

patterning techniques could enable the biogenic deposition of nanomaterial or cell-nanomaterial films in complex geometries[44–47]. Finally, with the *G. sulfurreducens* biofilms remaining electrochemically active following Pd(II) addition and biomineralization, these biofilms could ostensibly be used for repeated soluble Pd removal as planktonic *G. sulfurreducens* cells have been used in previous works[13]. Thus, such work opens the door to multiple avenues of investigation into fundamental and applied sustainable microbial-based technologies.

Author information

Corresponding author

Marko S. Chavez – Department of Physics and Astronomy, University of Southern California, Los Angeles, CA, 90089, USA; mschavez@usc.edu

Authors

Magdalene A. MacLean – Department of Physics and Astronomy, University of Southern California, Los Angeles, CA, 90089, USA

Mohamed Y. El-Naggar – Department of Physics and Astronomy, University of Southern California, Los Angeles, CA, 90089, USA; Department of Biological Sciences, University of Southern California, Los Angeles, CA, 90089, USA; Department of Chemistry, University of Southern California, Los Angeles, CA, 90089, USA

Author contributions

M.S.C. and M.Y.E.-N. designed the research; M.S.C. and M.A.M performed the research; M.S.C analyzed the data; M.S.C., M.A.M. and M.Y.E.-N. wrote and edited the manuscript.

Notes

The authors declare no conflict of interests.

Acknowledgments

This study was supported by the US Office of Naval Research Multidisciplinary University Research Initiative Grant No. N00014-18-1-2632. The authors would also like to thank the Core Center of Excellence in Nano Imaging at the University of Southern California.

References

(1) Myers, C. R.; Nealson, K. H. Bacterial Manganese Reduction and Growth with Manganese Oxide as the Sole Electron Acceptor. *Science.* **1988**, *240* (4857), 1319–1321.

(2) Lovley, D. R.; Stolz, J. F.; Nord Jr., G. L.; Phillips, E. J. P. Anaerobic Production of Magnetite by a Dissimilatory Iron-Reducing Microorganism. *Nature* **1987**, *330*, 252–254.

(3) Shi, L.; Dong, H.; Reguera, G.; Beyenal, H.; Lu, A.; Liu, J.; Yu, H. Q.; Fredrickson, J. K. Extracellular Electron Transfer Mechanisms between Microorganisms and Minerals. *Nat. Rev. Microbiol.* **2016**, *14* (10), 651–662. https://doi.org/10.1038/nrmicro.2016.93.

(4) Hartshorne, R. S.; Reardon, C. L.; Ross, D.; Nuester, J.; Clarke, T. A.; Gates, A. J.; Mills, P. C.; Fredrickson, J. K.; Zachara, J. M.; Shi, L.; Beliaev, A. S.; Marshall, M. J.; Tien, M.; Brantley, S.; Butt, J. N.; Richardson, D. J. Characterization of an Electron Conduit between Bacteria and the Extracellular Environment. *Proc. Natl. Acad. Sci. U. S. A.* **2009**, *106* (52), 22169–22174. https://doi.org/10.1073/pnas.0900086106.

(5) White, G. F.; Shi, Z.; Shi, L.; Wang, Z.; Dohnalkova, A. C.; Marshall, M. J.; Fredrickson, J. K.; Zachara, J. M.; Butt, J. N.; Richardson, D. J.; Clarke, T. A. Rapid Electron Exchange between Surface-Exposed Bacterial Cytochromes and Fe(III) Minerals. *Proc. Natl. Acad. Sci. U. S. A.* **2013**, *110* (16), 6346–6351. https://doi.org/10.1073/pnas.1220074110.

(6) Edwards, M. J.; White, G. F.; Butt, J. N.; Richardson, D. J.; Clarke, T. A. The Crystal Structure of

a Biological Insulated Transmembrane Molecular Wire. *Cell* **2020**, *181* (3), 665-673.e10. https://doi.org/10.1016/j.cell.2020.03.032.
(7) Chan, C. H.; Levar, C. E.; Jiménez-Otero, F.; Bond, D. R. Genome Scale Mutational Analysis of *Geobacter Sulfurreducens* Reveals Distinct Molecular Mechanisms for Respiration and Sensing of Poised Electrodes versus Fe(III) Oxides. *J. Bacteriol.* **2017**, *199* (19), 1–18. https://doi.org/10.1128/JB.00340-17.
(8) Zacharoff, L.; Ho, C.; Bond, D. R. Reduction of Low Potential Electron Acceptors Requires the CbcL Inner Membrane Cytochrome of *Geobacter Sulfurreducens*. *Bioelectrochemistry* **2016**, *107*, 7–13. https://doi.org/10.1016/j.bioelechem.2015.08.003.
(9) Peng, L.; Zhang, Y. Electrochimica Acta Cytochrome OmcZ Is Essential for the Current Generation by *Geobacter Sulfurreducens* under Low Electrode Potential. *Electrochim. Acta* **2017**, *228*, 447–452. https://doi.org/10.1016/j.electacta.2017.01.091.
(10) Zacharoff, L. A.; Morrone, D. J.; Bond, D. R. *Geobacter Sulfurreducens* Extracellular Multiheme Cytochrome PgcA Facilitates Respiration to Fe(III) Oxides but Not Electrodes. *Front. Microbiol.* **2017**, *8*, 1–11. https://doi.org/10.3389/fmicb.2017.02481.
(11) Otero, F. J.; Chan, C. H.; Bond, D. R. Identification of Different Putative Outer Membrane Electron Conduits Necessary for Fe(III) Citrate, Fe(III) Oxide, Mn(IV) Oxide, or Electrode Reduction by *Geobacter Sulfurreducens*. *J. Bacteriol.* **2018**, *200* (19), 1–20.
(12) Chadwick, G. L.; Jiménez Otero, F.; Gralnick, J. A.; Bond, D. R.; Orphan, V. J. NanoSIMS Imaging Reveals Metabolic Stratification within Current-Producing Biofilms. *Proc. Natl. Acad. Sci.* **2019**, *116* (41), 20716–20724. https://doi.org/10.1073/pnas.1912498116.
(13) Yates, M. D.; Cusick, R. D.; Logan, B. E. Extracellular Palladium Nanoparticle Production Using *Geobacter Sulfurreducens*. *ACS Sustain. Chem. Eng.* **2013**, *1* (9), 1165–1171. https://doi.org/10.1021/sc4000785.
(14) Pat-Espadas, A. M.; Razo-Flores, E.; Rangel-Mendez, J. R.; Cervantes, F. J. Direct and Quinone-Mediated Palladium Reduction by *Geobacter Sulfurreducens*: Mechanisms and Modeling. *Environ. Sci. Technol.* **2014**, *48* (5), 2910–2919. https://doi.org/10.1021/es403968e.
(15) Hernández-eligio, A.; Pat-espadas, A. M.; Vega-Alvarado, L.; Huerta-Amparan, M.; Cervantes, F. J.; Juárez, K. Global Transcriptional Analysis of *Geobacter Sulfurreducens* under Palladium Reducing Conditions Reveals New Key Cytochromes Involved. *Appl. Microbiol. Biotechnol.* **2020**, *104*, 4059–4069.
(16) Pat-Espadas, A. M.; Razo-Flores, E.; Rangel-Mendez, J. R.; Cervantes, F. J. Reduction of Palladium and Production of Nano-Catalyst by *Geobacter Sulfurreducens*. *Appl. Microbiol. Biotechnol.* **2013**, *97* (21), 9553–9560. https://doi.org/10.1007/s00253-012-4640-9.
(17) Tuo, Y.; Liu, G.; Zhou, J.; Wang, A.; Wang, J.; Jin, R.; Lv, H. Microbial Formation of Palladium Nanoparticles by *Geobacter Sulfurreducens* for Chromate Reduction. *Bioresour. Technol.* **2013**, *133*, 606–611. https://doi.org/10.1016/j.biortech.2013.02.016.
(18) Torborg, C.; Beller, M. Recent Applications of Palladium-Catalyzed Coupling Reactions in the Pharmaceutical, Agrochemical, and Fine Chemical Industries. *Adv. Synth. Catal.* **2009**, *351*, 3027–3043. https://doi.org/10.1002/adsc.200900587.
(19) Chen, Y.; Qiao, Q.; Cao, J.; Li, H.; Bian, Z. Precious Metal Recovery. *Joule* **2021**, *5* (12), 3097–3115. https://doi.org/10.1016/j.joule.2021.11.002.
(20) Chen, A.; Ostrom, C. Palladium-Based Nanomaterials: Synthesis and Electrochemical Applications. *Chem. Rev.* **2015**, *115* (21), 11999–12044. https://doi.org/10.1021/acs.chemrev.5b00324.
(21) McFarlane, I. R.; Lazzari-Dean, J. R.; El-Naggar, M. Y. Field Effect Transistors Based on Semiconductive Microbially Synthesized Chalcogenide Nanofibers. *Acta Biomater.* **2015**, *13*, 364–373. https://doi.org/10.1016/j.actbio.2014.11.005.
(22) Wu, J. W.; Ng, I. S. Biofabrication of Gold Nanoparticles by *Shewanella* Species. *Bioresour. Bioprocess.* **2017**, *4* (1). https://doi.org/10.1186/s40643-017-0181-5.
(23) De Corte, S.; Hennebel, T.; De Gusseme, B.; Verstraete, W.; Boon, N. Bio-Palladium: From Metal

Recovery to Catalytic Applications. *Microb. Biotechnol.* **2012**, *5* (1), 5–17. https://doi.org/10.1111/j.1751-7915.2011.00265.x.

(24) Shedbalkar, U.; Singh, R.; Wadhwani, S.; Gaidhani, S.; Chopade, B. A. Microbial Synthesis of Gold Nanoparticles: Current Status and Future Prospects. *Adv. Colloid Interface Sci.* **2014**, *209*, 40–48. https://doi.org/10.1016/j.cis.2013.12.011.

(25) Estroff, L. A. Introduction: Biomineralization. *Chem. Rev.* **2008**, *108* (11), 4329–4331. https://doi.org/10.1021/cr8004789.

(26) Meldrum, F. C.; Co, H. Controlling Mineral Morphologies and Structures in Biological and Synthetic Systems. *Chem. Rev.* **2008**, *11*, 4332–4432.

(27) Kimber, R. L.; Lewis, E. A.; Parmeggiani, F.; Smith, K.; Bagshaw, H.; Starborg, T.; Joshi, N.; Figueroa, A. I.; van der Laan, G.; Cibin, G.; Gianolio, D.; Haigh, S. J.; Pattrick, R. A. D.; Turner, N. J.; Lloyd, J. R. Biosynthesis and Characterization of Copper Nanoparticles Using *Shewanella Oneidensis*: Application for Click Chemistry. *Small* **2018**, *14* (10), 1–8. https://doi.org/10.1002/smll.201703145.

(28) Chellamuthu, P.; Tran, F.; Silva, K. P. T.; Chavez, M. S.; El-Naggar, M. Y.; Boedicker, J. Q. Engineering Bacteria for Biogenic Synthesis of Chalcogenide Nanomaterials. *Microb. Biotechnol.* **2018**, *12* (1), 161–172. https://doi.org/10.1111/1751-7915.13320.

(29) Chellamuthu, P.; Naughton, K.; Pirbadian, S.; Silva, K. P. T.; Chavez, M. S.; El-naggar, M. Y.; Boedicker, J. Biogenic Control of Manganese Doping in Zinc Sulfide Nanomaterial Using *Shewanella Oneidensis* MR-1. *Front. Microbiol.* **2019**, *10* (May), 1–10. https://doi.org/10.3389/fmicb.2019.00938.

(30) Tanzil, A. H.; Sultana, S. T.; Saunders, S. R.; Dohnalkova, A. C.; Shi, L.; Davenport, E.; Ha, P.; Beyenal, H. Production of Gold Nanoparticles by Electrode-Respiring *Geobacter Sulfurreducens* Biofilms. *Enzyme Microb. Technol.* **2016**, *95*, 69–75. https://doi.org/10.1016/j.enzmictec.2016.07.012.

(31) Ng, C. K.; Karahan, H. E.; Loo, S. C. J.; Chen, Y.; Cao, B. Biofilm-Templated Heteroatom-Doped Carbon-Palladium Nanocomposite Catalyst for Hexavalent Chromium Reduction. *ACS Appl. Mater. Interfaces* **2019**, *11* (27), 24018–24026. https://doi.org/10.1021/acsami.9b04095.

(32) Flemming, H.; Wingender, J. The Biofilm Matrix. *Nat. Publ. Gr.* **2010**, *8* (August). https://doi.org/10.1038/nrmicro2415.

(33) Marsili, E.; Rollefson, J. B.; Baron, D. B.; Hozalski, R. M.; Bond, D. R. Microbial Biofilm Voltammetry: Direct Electrochemical Characterization of Catalytic Electrode-Attached Biofilms. *Appl. Environ. Microbiol.* **2008**, *74* (23), 7329–7337. https://doi.org/10.1128/AEM.00177-08.

(34) Bonanni, P. S.; Bradley, D. F.; Schrott, G. D.; Pablo, J. Limitations for Current Production in *Geobacter Sulfurreducens* Biofilms. *ChemSusChem* **2013**, *6*, 711–720. https://doi.org/10.1002/cssc.201200671.

(35) Sun, D.; Chen, J.; Huang, H.; Liu, W.; Ye, Y. The Effect of Biofilm Thickness on Electrochemical Activity of *Geobacter Sulfurreducens*. *Int. J. Hydrogen Energy* **2016**, *41* (37), 16523–16528. https://doi.org/10.1016/j.ijhydene.2016.04.163.

(36) Elgrishi, N.; Rountree, K. J.; McCarthy, B. D.; Rountree, E. S.; Eisenhart, T. T.; Dempsey, J. L. A Practical Beginner's Guide to Cyclic Voltammetry. *J. Chem. Educ.* **2018**, *95* (2), 197–206. https://doi.org/10.1021/acs.jchemed.7b00361.

(37) Torres, C. I.; Marcus, A. K.; Lee, H. S.; Parameswaran, P.; Krajmalnik-Brown, R.; Rittmann, B. E. A Kinetic Perspective on Extracellular Electron Transfer by Anode-Respiring Bacteria. *FEMS Microbiol. Rev.* **2010**, *34* (1), 3–17. https://doi.org/10.1111/j.1574-6976.2009.00191.x.

(38) Zacharoff, L. A.; El-Naggar, M. Y. Redox Conduction in Biofilms: From Respiration to Living Electronics. *Curr. Opin. Electrochem.* **2017**, *4* (1), 182–189. https://doi.org/10.1016/j.coelec.2017.09.003.

(39) Chen, Y.; Chen, Y. Difference in Toxicity of Pd (II) and Mechanism of Action before and after Reduction by *Bacillus Wiedmannii* MSM. *Environ. Sci. Pollut. Res.* **2021**, No. Ii. https://doi.org/10.1007/s11356-021-15736-y.

(40) Gadd, G. M. Metals and Microorganisms: A Problem of Definition. *FEMS Microbiol. Lett.* **1992**, *100*, 197–203. https://doi.org/10.1016/0378-1097(92)90209-7.
(41) Alberts, B.; Johnson, A.; Lewis, J.; Raff, M.; Robert, K.; Walter, P. *Molecular Biology of The Cell*, 4th ed.; 2002.
(42) Snider, R. M.; Strycharz-Glaven, S. M.; Tsoi, S. D.; Erickson, J. S.; Tender, L. M. Long-Range Electron Transport in *Geobacter Sulfurreducens* Biofilms Is Redox Gradient-Driven. *Proc. Natl. Acad. Sci.* **2012**, *109* (38), 15467–15472. https://doi.org/10.1073/pnas.1209829109.
(43) Yates, M. D.; Golden, J. P.; Roy, J.; Strycharz-Glaven, S. M.; Tsoi, S.; Erickson, J. S.; El-Naggar, M. Y.; Calabrese Barton, S.; Tender, L. M. Thermally Activated Long Range Electron Transport in Living Biofilms. *Phys. Chem. Chem. Phys.* **2015**, *17* (48), 32564–32570. https://doi.org/10.1039/c5cp05152e.
(44) Zhao, F.; Chavez, M. S.; Naughton, K. L.; Cole, C. M.; Gralnick, J. A.; El-Naggar, M. Y.; Boedicker, J. Q. Light-Induced Patterning of Electroactive Bacterial Biofilms. *bioRxiv* **2021**, 2021.12.20.473588.
(45) Catania, C.; Karbelkar, A. A.; Furst, A. L. Engineering the Interface between Electroactive Bacteria and Electrodes. *Joule* **2021**, *5* (4), 743–747. https://doi.org/10.1016/j.joule.2021.02.001.
(46) Furst, A. L.; Smith, M. J.; Lee, M. C.; Francis, M. B. DNA Hybridization to Interface Current-Producing Cells with Electrode Surfaces. *ACS Cent. Sci.* **2018**, *4* (7), 880–884. https://doi.org/10.1021/acscentsci.8b00255.
(47) Young, T. D.; Liau, W. T.; Lee, C. K.; Mellody, M.; Wong, G. C. L.; Kasko, A. M.; Weiss, P. S. Selective Promotion of Adhesion of *Shewanella Oneidensis* on Mannose-Decorated Glycopolymer Surfaces. *ACS Appl. Mater. Interfaces* **2020**, *12* (32), 35767–35781. https://doi.org/10.1021/acsami.0c04329.

623

624 **For Abstract Graphic Only**

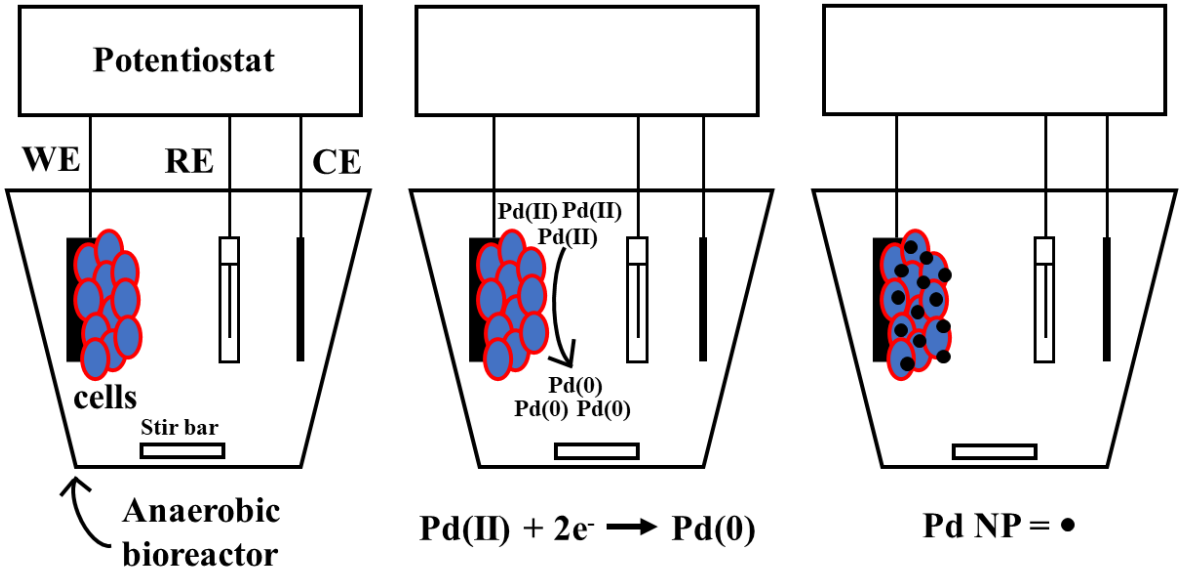

625